Environment International 131 (2019) 105005

Contents lists available at ScienceDirect

Environment International

journal homepage: www.elsevier.com/locate/envint

Mechanistic understanding of the NOB suppression by free ammonia inhibition in continuous flow aerobic granulation bioreactors

Timothy R. Kent[a,1], Yewei Sun[a], Zhaohui An[a], Charles B. Bott[b], Zhi-Wu Wang[a,*]

[a] Occoquan Laboratory, Department of Civil and Environmental Engineering, Virginia Tech, 9408 Prince William Street, Manassas, VA 20110, USA
[b] Hampton Roads Sanitation District, 1434 Air Rail Avenue, Virginia Beach, VA 23455, USA

ARTICLE INFO

Handling Editor: Guo-ping Sheng

Keywords:
Free ammonia
Granule size
AOB:NOB
Partial nitritation
Continuous flow
Diffusion limitation

ABSTRACT

A partial nitritation continuous flow reactor (CFR) was operated for eight months demonstrating that partial nitritation granular sludge can remain stable under continuous flow conditions. The ammonia oxidizing bacteria (AOB)-to-nitrite oxidizing bacteria (NOB) activity ratios were determined for a series of granule sizes to understand the impact of mass diffusion limitation on the free ammonia (FA) inhibition of NOB. When dissolved oxygen (DO) limitation is the only mechanism for NOB suppression, the AOB:NOB ratio was usually found to increase with the granule size. However, the trend is reversed when FA has an inhibitory effect on NOB, as was observed in this study. The decrease in AOB:NOB ratio indicates that smaller granules, e.g. diameter < 150 μm, are preferred for nitrite accumulation when high FA concentration is present, as in the partial nitritation process. The trend was further verified by observing the increase in the apparent inhibition coefficient as granule size increased. Indeed, this study for the first time quantified the effect of diffusion limitation on the apparent inhibition coefficient of NOB in aerobic granules. A mathematical model was then utilized to interpret the observed suppression of NOB and predicted that NOB suppression was only complete at the granule surface. The NOB that did survive in larger granules was forced to dwell within the granule interior, where the AOB growth declines due to DO diffusion limitation. This means FA inhibition can be taken advantage of as an effective means for NOB suppression in small granules or thin biofilms. Further, both FA inhibition and DO limitation were found to be required for the suppression of NOB in mainstream aerobic granules.

1. Introduction

Traditional nitrogen removal in wastewater treatment plants has been carried out through the nitrification and denitrification processes which requires both external carbon source addition and intensive aeration energy input (Ma et al., 2016). A current trend in wastewater research is to achieve significant savings in energy and chemical costs by developing shortcut nitrogen removal processes, where NO_2^- is accumulated by the suppression of nitrite oxidizing bacteria (NOB). This accumulated NO_2^- may be converted directly to N_2 gas by denitrification heterotrophic organisms through nitrite shunt (Nogaj et al., 2014), or in the presence of excess NH_4^+, through deammonification by anaerobic ammonia oxidizing bacteria, namely anammox (AMX) (Xu et al., 2015). Both of these processes require the suppression of NOB, and several strategies have been suggested, including solids retention time (SRT) control, dissolved oxygen (DO) limitation, and bioaugmentation of ammonia oxidizing bacteria (AOB) (Xu et al., 2015). One method of note for NOB suppression is free ammonia (FA) inhibition. At sufficiently high levels, FA has been shown to selectively inhibit NOB without negatively impacting the growth of AOB. Implementation of such a strategy has been successful in sidestream treatment of reject wastewater (Cao et al., 2017; Gu et al., 2007). It is unclear, however, if FA inhibition may be used effectively under mainstream conditions, i.e. continuous flow, low temperature, and low FA concentrations.

Another research trend is the rising interest in granular sludge for wastewater treatment (Kent et al., 2018). Aerobic granules are dense conglomerates of self-aggregating microorganisms with good settleablilty, compact structure, and smooth, round surfaces (Kent et al., 2018). Aerobic granulation has been observed in sequential batch reactors (SBRs) for many years, and research is now being focused on their stability in continuous flow reactors (CFRs) (Kent et al., 2018; Sun et al., 2019). Granular sludge allows for the development of a stratified internal structure with different microbial communities inhabiting different layers. This phenomenon of different functional groups

* Corresponding author.
E-mail address: wzw@vt.edu (Z.-W. Wang).
[1] AECOM, 10 S Jefferson St, Roanoke, VA 24011, USA.

https://doi.org/10.1016/j.envint.2019.105005
Received 11 May 2019; Received in revised form 1 July 2019; Accepted 9 July 2019
Available online 19 July 2019

arranging in coherent layers is largely explained by the profiles of DO and substrate, as they diffuse towards the granule interior.

There have been some studies demonstrating FA inhibition of NOB in granules and biofilms (Wei et al., 2017; Wei et al., 2018), however, discussion of the role of mass diffusion limitation in these systems is currently missing from the literature. FA inhibition studies have generally been focused on flocculent sludge (Hiatt and Grady, 2008; Wu et al., 2016), and it is not yet clear how a granular structure may influence the inhibitory levels of FA. Granular sludge is larger and more compact than flocculent sludge, leading to internal resistances to the diffusion of substrates necessary for nitrogen removal. This diffusion resistance was observed by Piculell et al. (2016) who exposed biofilms with thickness of 50 and 400 μm to reject water. Nitrite accumulation by inhibition of NOB was noted to be more successful in the thinner biofilms in their study. Although many parameters were variable in this study, the results suggest that diffusion did play a role in FA inhibition of NOB in biofilms. However, this study did not seek to establish useful parameters in quantifying the effect of FA, e.g. an inhibition constant. Even when the ammonia inhibition constant has been determined for granular sludge, such as in the study by Cui et al. (2017), the influence of diffusion has not been taken into consideration.

This study looks into the possibility of leveraging FA as a mechanism for particle size-dependent NOB suppression in granules and its potential role in determining the best size of granules that should be used for the mainstream partial nitritation. It is our hypothesis that the effectiveness of FA inhibition-enabled NOB suppression is granule size-dependent in that the mass diffusion limitation would allow NOB to survive in the granule interior while AOB dominates at the surface. This hypothesis was tested in this study by evaluating the impact of granule size on the activity ratios of AOB-to-NOB, as well as the effect on the apparent inhibition coefficient of FA. These experimental results were then compared with those from mathematical model prediction to provide mechanistic insights to the potential of FA inhibition-enabled NOB suppression in mainstream application.

2. Materials and methods

2.1. Reactor setup and operation

The partial nitritation reactor in Fig. 1a comprised an upflow, 1.5 L airlift reactor (ALR). The reactor diameter was 6 cm with a 3 cm diameter riser tube. A three-phase separator was provided at the top of the reactor near the effluent port to retain granular sludge (Fig. 1b). Influent was fed from a chilled reservoir by means of a peristaltic pump. The ALR was seeded with granular sludge cultivated in a DEMON® reactor operated by Hampton Roads Sanitation District (HRSD), Virginia Beach, VA. The ALR was operated under the continuous flow mode with a hydraulic retention time (HRT) of approximately 5.2 h. The medium used for each batch experiment comprised approximately (per 1 L) 50 mg NH_3-N, 1100 mg $NaHCO_3$, 350 mg Na_2HPO_4, 75 mg NaH_2PO_4, and trace elements as described in the study by Poot et al. (2016). The gas flow rates from an air pump and a N_2 gas cylinder were manually adjusted to maintain an average DO < 1 mg L^{-1} in the ALR. The reactor temperature was averaged at 20.6 °C in a temperature-controlled room.

2.2. Analytical methods

Nitrogen concentrations of NH_4^+, NO_2^-, and NO_3^- were measured using the Hach salicylate/cyanurate, NitriVer 3, and TNTplus 835 kits according to standard methods (Reardon et al., 1966; USEPA, 2017). DO was measured every 30 min by a submersed, luminescent DO probe (Hach, Intellical™ LDO101, Loveland, CO, USA). The turbidity was determined using a turbidity meter (Hach, 2100 N, Loveland, CO, USA). The particle size distribution was analyzed using a laser scattering particle size analyzer (Horiba, LA-950, Kyoto, Japan). A Nikon Eclipse E200 microscope (Melville, NY, USA) was utilized to take microscopic images of aerobic granule morphology.

2.2.1. AOB:NOB activity ratio measurement for various size granules

In order to understand the granule size effect on AOB and NOB activities, granular sludge from the partial nitritation reactor in Fig. 1 was passed through a series of sieves to separate the biomass into distinct size ranges as follows (in μm): 106–149, 149–250, 250–297, 297–350, 350–420, and 420–500. The sludge in each size range was subsequently resuspended in a suspension medium comprising approximately (per 1 L): 500 mg $NaHCO_3$, 35 mg NaH_2PO_4, and trace elements as described in Poot et al. (2016). The suspended sludge was incubated for at least 1 h on a shaker plate to completely consume any residual substrate from the ALR. Then, the granules and solution were transferred to 70 mL BOD bottles on a stir plate operating at 80 to 100 rpm. BOD probes (Hach, Intellical™ LBOD101, Loveland, CO, USA) were inserted into the BOD bottles and sealed with grease to ensure that DO was not transferred from the environment by means of leaking. The pH of the medium was maintained in the range of 7.8–8.0, which is optimal for both *Nitrospira* and *Nitrobacter* (Blackburne et al., 2007; Grunditz and Dalhammar, 2001), allowing the maximum activity of NOB. The initial DO in the bottles was maintained in the range of 7–8 mg L^{-1} to ensure non-limiting oxygen conditions. The AOB and NOB activities were quantified by measuring the oxygen uptake rate (OUR, mg O_2 L^{-1} h^{-1}) in a modified procedure similar to that used in the study by Moussa et al. (2003). Briefly, the drop of DO with time was

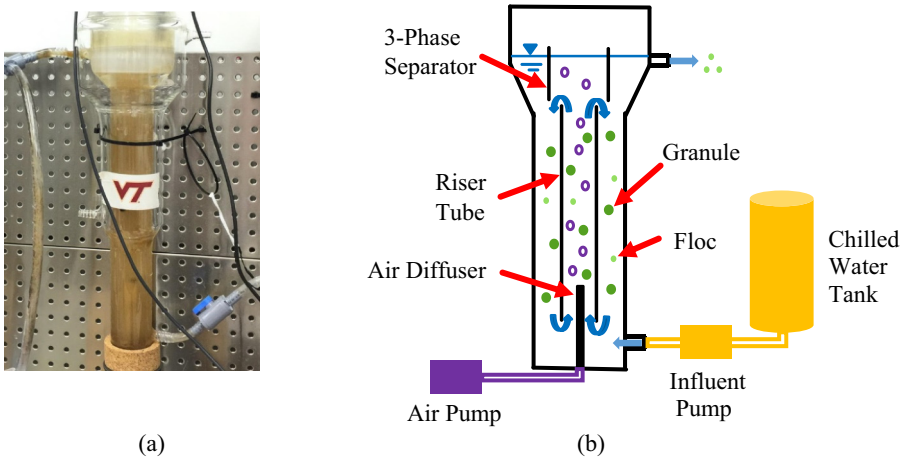

Fig. 1. ALR used in this study: (a) photographic and (b) schematic illustration.

measured every minute for 15 min to establish the endogenous OUR, namely OUR_1. After that, $NaNO_2$ was spiked into the BOD bottle to achieve an initial concentration of approximately 100 mg NO_2^--N L^{-1}. Using 100 mg NO_2^--N L^{-1} (0.004 mg HNO_2-N L^{-1} at pH = 7.8 and T = 20 °C) maintains nitrite non-limiting conditions while keeping the HNO_2 well below the threshold inhibitory value of 0.011 mg HNO_2-N L^{-1} (Ge et al., 2015). The DO was again monitored and used to calculate the OUR, namely OUR_2. Then, NH_4Cl was dosed to the bottle to ensure approximately 100 mg N L^{-1} initial concentration was achieved, and DO was again monitored to provide an OUR_3. The following equations provide the estimation of endogenous respiration rate, as well as AOB and NOB oxygen utilization rates, based on this experimental design.

$$OUR_{endo} = OUR_1 \quad (1)$$

$$OUR_{NOB} = OUR_2 - OUR_1 \quad (2)$$

$$OUR_{AOB} = OUR_3 - OUR_{NOB} - OUR_1 \quad (3)$$

For easy comparison, OURs of both AOB and NOB were converted to their relevant nitrogen utilization rates using the stoichiometric coefficients of 3.43 g O_2 g-1 NH_4^+-N and 1.14 g O_2 g^{-1} NO_2^--N (Ma et al., 2016), respectively. Although AOB and NOB activities are individually dependent on the biomass concentration, the ratio of the two cancels out the biomass effect. This allows for the AOB:NOB ratios to be compared between the samples of different granules sizes even though the samples differed in biomass concentration.

2.2.2. Granule size effect on free ammonia inhibition coefficient

Although the granule size effect on the FA inhibition of NOB can be indirectly inferred from the OUR_{NOB}, a more direct measurement of the FA inhibition can be determined by the apparent FA inhibition constant, namely $K_{I,FAapp}$ (mg N L^{-1}). To determine $K_{I,FAapp}$, a sample from each granule size range was taken and placed in BOD bottles containing 250 mL of suspension solution with approximately 100 mg N L^{-1} of initial nitrite concentration. For each granule size, the bottle was placed on a shaker to ensure good mixing. 2.5 mL samples were taken from the bottle before and after 30 min incubation to establish the baseline for uninhibited NOB activity based on the difference in NO_3^- concertation. Then, approximately 25 mg N L^{-1} ammonia was added and 2.5 mL samples was taken before and after another 30 to 40 min reaction period. Intensive aeration was supplied throughout the experimental duration to ensure DO is not the rate-limiting factor. NO_3^-, NH_4^+, T, and pH were measured for each sample to determine FA and NO_3^- conversion rates.

These steps were repeated for 50 mg L^{-1} of ammonium. The difference in NO_3^- observed over the reaction period allowed for the computation of the nitrate production rate, namely R_{NO3}. The bulk FA for each period was calculated using the average of the initial and final TAN values, T, pH, and Eqs. (4) to (6) from Metcalf and Eddy (2014).

$$R_{NO3} = \frac{C_{NO_3^-} - C^o_{NO_3^-}}{t_R} \quad (4)$$

$$\overline{C_{FA}} = \frac{C_{FA} + C^o_{FA}}{2} \quad (5)$$

$$C_{FA} = \frac{C_{TAN}(10^{pH})}{\exp\left(\frac{6334}{273+T}\right) + 10^{pH}} \quad (6)$$

in which $C_{NO_3^-}{}^o$ and $C_{NO_3^-}$ represent the initial and final nitrate concentrations in mg N L^{-1}, respectively, after reaction time (t_R). Likewise, $C_{FA}{}^o$ and C_{FA} represent the initial and final FA concentrations mg N L^{-1}. C_{TAN} stands for the TAN concentration in mg N L^{-1}. Further, the apparent FA inhibition constant, $K_{I,FAapp}$, can be determined by assuming an uncompetitive inhibition model, which is commonly used in the literature (Park and Bae, 2009; Gee et al., 1990). Eq. (7) was adapted from Park and Bae (2009) to model this type of inhibition, using the nitrite oxidation rate determined at each of the average FA concentrations.

$$\frac{R^o_{NO_3^-}}{R_{NO_3^-}} = \left(\frac{\overline{C_{FA}}}{K_{I,FAapp}} + 1\right) \quad (7)$$

in which $R_{NO_3^-}{}^o$ is the initial, uninhibited nitrite oxidation rate in mg N L^{-1} min^{-1}. Plotting $\frac{R^o_{NO_3^-}}{R_{NO_3^-}}$ as a function of $\overline{C_{FA}}$, followed by linear regression, provides the value of $K_{I,FAapp}$ for each granule size range.

2.3. Model development

An explanation for the observed AOB:NOB activity ratios was obtained by implementing a biofilm model adapted from the work by Li et al., 2019. The model was programmed in MathWorks® MatLab (R2018a). Simulations were run to predict the distribution profiles of AOB, NOB, NH_4^+, NO_2^-, NO_3^-, FA, and DO in granular sludge with various particle size. Average radii were used as representative of each size range from Section 2.2.1. In this way two scenarios were considered, specifically the operation with and without FA inhibition of NOB. A regressed true FA inhibition coefficient, $K_{I,FA}$, was used in Eq. (S3) in Table S1 to show the impact of FA. The case without FA inhibition was achieved by setting $S_{FA}/K_{I,FA}$ at zero, which reduces Eq. (S3) to the standard Monod equation.

2.3.1. Microbial kinetics and substrate utilization

The equations, stoichiometry matrix, and parameters for microbial kinetics and substrate utilization are summarized in Tables S1 to S3, respectively. Temperature sensitive parameters were converted to values at the average operating temperature of the reactor, i.e. 20.6 °C, by using Eq. (8), where μ_T is the maximum growth rate at temperature T in Kelvin, μ_{293} is the maximum growth rate at 293 Kelvin, and θ is the temperature coefficient. Eq. (8) was taken from the work of Hao et al. (2002a), along with the values of θ for AOB, NOB, and AMX. A similar equation is used for the decay coefficient, b.

$$\mu_T = \mu_{293} e^{[-\theta(293-T)]} \quad (8)$$

Monod kinetics were assumed for bacterial growth, although the expression for NOB was modified to account for inhibition in Eq. (S3). Given the FA inhibitory threshold for AOB is 7 to 150 mg NH_3 L^{-1} (Anthonisen et al., 1976), the model is simplified by assuming FA inhibition of AOB is negligible. Although AMX is known to produce NO_3^-, its contribution is considered negligible compared to the contribution of NOB in this study in view of the negligible amount of AMX present in the system, as can be inferred from the N balance in Table 1. The kinetic parameters of AMX relating to NO_3^- production, therefore, are omitted in Tables S1 to S3. Since no COD was provided to the ALR, heterotrophic bacteria were not considered in the model.

2.3.2. Effect of diffusion on substrate species concentrations within the granule structure

The diffusivity of each chemical species was assumed to be 80% their values in water as listed in Table S3 according to the study by Sen and Randall (2008). The diffusion in granules from each size range was

Table 1
Four-month average bulk concentrations and temperature measured in the partial nitritation ALR.

Variable	Value	Unit
NH_4^+	21.7 ± 3.7	g N m^{-3}
NO_2^-	20.8 ± 3.4	g N m^{-3}
NO_3^-	3.4 ± 0.7	g N m^{-3}
DO	0.76 ± 0.02	g m^{-3}
T	20.6 ± 0.01	°C
pH	7.8	–

accounted for in the model by dividing the granules into 21 layers. The steady state mass balance between diffusion and reaction in each spherical layer is modeled in Eq. (9).

$$D_i\left(\frac{d^2C_i}{dr^2}+\frac{2}{r}\frac{dC_i}{dr}\right)-R_i=0 \quad (9)$$

in which D_i is the diffusivity of substrate i, C_i is the concentration of substrate i, r is the distance from the granule center, and R_i is the utilization rate of substrate i. The thickness of boundary layer at the surface of each granule was considered negligible for the intensive mixing in the bioreactors. Further, biomass concentrations and distribution in each granule is determined solely by steady state substrate distribution, i.e. diffusion of biomass and attachment/detachment mechanisms were not considered in the model.

The CO_2/HCO_3^- buffer system was assumed to be the controlling factor for changes in pH along the granule radius. In this manner, pH could be simply calculated at each point in the granule by using Eq. (10)

$$pH=pH^o-\log\left(K\frac{C_{CO_2}}{C_{HCO_3^-}}\right) \quad (10)$$

where pH^o represents the bulk pH, and K is the equilibrium constant for the CO_2/HCO_3^- (mole/mol) system and equal to $10^{-6.3}$ (Jensen, 2003). The consumption of alkalinity, i.e. HCO_3^-, is assumed to be due solely to ammonium oxidation according to Table S2. The H^+ produced by AOB is assumed to be immediately consumed by alkalinity, eliminating the need to consider diffusion of H^+ in the model.

3. Results

3.1. Steady-state performance of the partial nitritation ALR

The steady-state effluent concentrations from the reactor are shown in Table 1. The almost equal concentrations between NH_4^+-N and NO_2^--N indicated effective suppression of NOB by FA which is around 0.57 mg NH_3 L^{-1} at an average pH of 7.8 and temperature of 20.6 °C. A low DO/TAN ratio = 0.04, was maintained and thus verified as one of the effective operational strategies for suppressing NOB activity. The combined total nitrogen concentrations in the effluent yielded an average TN of 45.9 mg N L^{-1} (Table 1), somewhat less than the total input TAN (50 mg N L^{-1}). The difference in nitrogen content suggests there might be some AMX activity since the absence of COD prevented the growth of denitrifiers. This supports incorporating AMX in the model for biomass growth in the granular sludge (Tables S1 to S3).

The partial nitritation reactor was operated for eight months by the conclusion of this study. The granule size distribution, granule morphology, and ALR effluent turbidity were analyzed. Fig. 2 shows that majority of the granules were stabilized between 100 and 400 μm with a mean diameter of 247 μm. The images of granules from each size range, as shown in Fig. 3, display that the granules had well-defined, round shapes with smooth surfaces. The turbidity of the effluent was determined to be only 2.3 NTU, evidencing the good retention of biomass and integrity of the granular sludge.

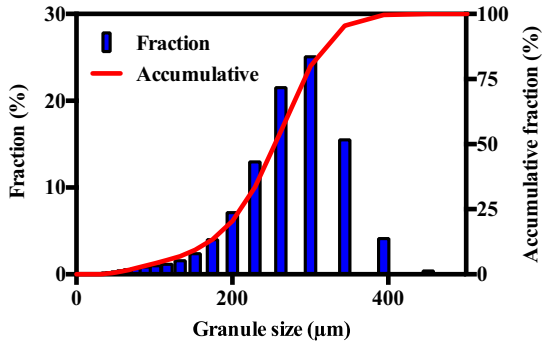

Fig. 2. Particle size distribution for the partial nitritation ALR at the end of eight-month operation.

3.2. Effect of granule size on AOB:NOB activity ratios

The activity ratios of AOB to NOB were determined according to Eqs. (1) to (3) based on their respective oxygen utilization rates in each granule size. As can be seen in Fig. 4, the smallest granules (e.g. 127.5 μm) possessed the highest AOB-to-NOB activity ratio of 252.3. As the granule size increases to 199.5 μm, this ratio dramatically dropped to 38.5. With the granule size further increasing to 460 μm, the AOB-to-NOB activity ratio dropped to as low as 4.6. It is noteworthy that this negative effect of granule size on AOB:NOB activity ratio is contrary to the observation in the literature when FA inhibition was not present (Zhu et al., 2018; Winkler et al., 2011).

3.3. Effect of granule size on the apparent FA inhibition coefficient

It is our hypothesis that the inversed relationship between granule size and AOB:NOB activity ratio might be ascribed to the mass diffusion effect combined with the FA inhibition, which can be quantified by the apparent FA inhibition coefficient, namely $K_{I,FAapp}$, according to the method using Eq. (7). Fig. 5 shows that the $K_{I,FAapp}$ is actually positively related to the granule sizes, i.e., the 127.5 μm granules possessed the smallest $K_{I,FAapp}$ value of 2.4 mg N L^{-1}. As the granule sizes increased to 385 μm, the $K_{I,FAapp}$ value increased to as high as 16.2 mg N L^{-1}. These experimentally determined $K_{I,FAapp}$ values actually have taken the diffusion effect into consideration according to Eq. (7). Consequently, large granules are expected to exhibit more mass diffusion resistance and thus augment the values of $K_{I,FAapp}$, which is in line with the trend observed in Fig. 5. This further supports the conclusion that diffusion limits the effectiveness of FA inhibition of NOB in large granules, which may explain the negative effect of granule size on AOB:NOB activity ratios as observed in Fig. 4.

3.4. Model simulation of the effect of granule size on AOB:NOB ratios with and without FA inhibition

The mathematical model described in Tables S1 and S2 was calibrated with the oxygen utilization rate-based AOB:NOB activity ratios measured in Fig. 4. The good agreement between the model-predicted and experimentally-measured data in Fig. 4 indicates the soundness of equations in Table S1 in description of the granule size effect on AOB:NOB activity ratios. Based on the experimental results in Figs. 4 and 5, it is our hypothesis that the AOB's outcompetition of NOB under FA inhibition might have been attenuated by the shielding effect of granule size. To test this hypothesis, we compared the model prediction of the granule size effect on AOB:NOB ratio with and without FA inhibition. The calibrated model with parameters listed in Table S3 was used to predict the scenario with FA inhibition. As can be seen in Fig. 6, totally opposite trends were predicted under the two scenarios. The increase of AOB:NOB ratio with increasing granule size in Fig. 6 actually has been broadly observed previously when FA inhibition was not present (Zhu et al., 2018; Winkler et al., 2011).

3.5. Model simulation of the diffusion profiles and mass distribution within aerobic granules

Since the primary distinction between granules of different sizes is their resistance to the transport of substrate and DO, diffusion should have a key role in determining the relative activities and abundance of AOB and NOB. Fig. 7 shows the impact of diffusion of the relevant mass species along the granule radius at steady state described in Table 1. It can be seen that the concentration profiles of DO and NH_4^+ both

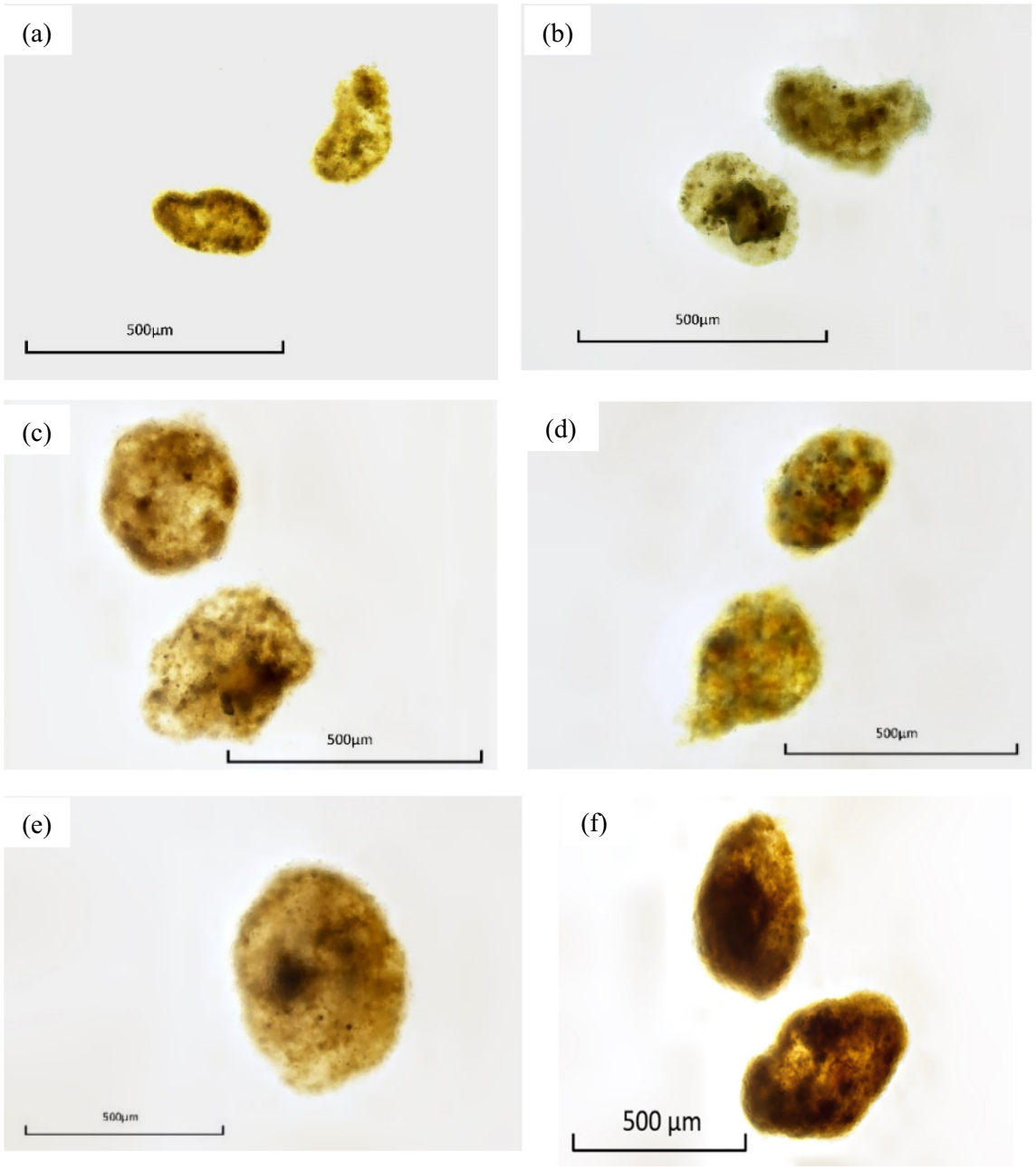

Fig. 3. Images of the granule morphology for each size range tested. (a) 106–150 μm, (b) 150–250 μm, (c) 250–297 μm, (d) 297–350 μm, (e) 350–420 μm, and (f) 420–500 μm.

decrease along the granule radius for each size modeled. This decline is steepest within the 50 μm near the granule surface. Beyond this depth, most of the DO is depleted. This result is consistent with the AOB profiles in Fig. 8, where AOB is most prevalent in the top 50 μm layer of the granules. The NO_2^- profiles for each granule size in Fig. 7 are nearly identical, i.e., increasing within the 50 μm near the surface, corresponding to the abundance of AOB, and then flattening out towards the granule center. Such behavior indicates limited NOB activity. Accordingly, only a slight increase of NO_3^- concentration towards the granule center is observed as the granule size increases beyond 99.75 μm (Fig. 7). Almost no NOB activity can be seen in the smallest granule size, i.e. having a radius of 63.75 μm. It is noteworthy that in all different size granules, the AOB cell concentration in the aerobic granules is about two orders of magnitude greater than that of the NOB cells throughout the granules (Fig. 8).

AOB has the higher DO affinity (K_{O2} = 0.2 mg L^{-1}) and is favored over NOB (K_{O2} = 0.4 mg L^{-1}) at lower DO concentrations (Table S3), especially within the granule interior, where DO is at its lowest, i.e. below 0.1 mg L^{-1} (Fig. 7). In fact, concentration profiles from the model simulation indicate nearly complete depletion of DO in granules having a diameter > 150 μm, i.e. it is only 5% of its bulk concentration after penetrating to approximately 50 μm under the granule surface (Fig. 7). The impact of DO limitation on NOB is evident since a peak in NOB's abundance is also observed at a similar depth, about 60 μm below the granule surface (Fig. 8). The low concentration of DO approximately 50 μm deep within the granule suppresses the ability of NOB to grow, leading to a sharply decreasing trend of NOB abundance further inside the granule. DO limitation, however, should not be the only factor influencing the relative activities of AOB and NOB since there are sufficient concentrations of NO_2^- and DO for NOB to grow and compete with AOB in the 50-μm top layer of the granules (Figs. 7 and 8). The prediction of NOB abundance peaking only 60 μm below

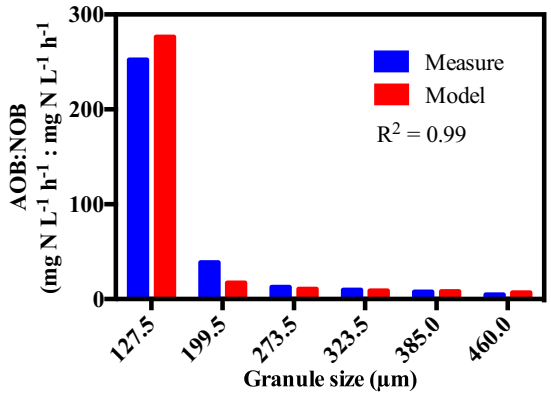

Fig. 4. Model simulated and experimentally measured AOB:NOB activity ratios for tested granule sizes.

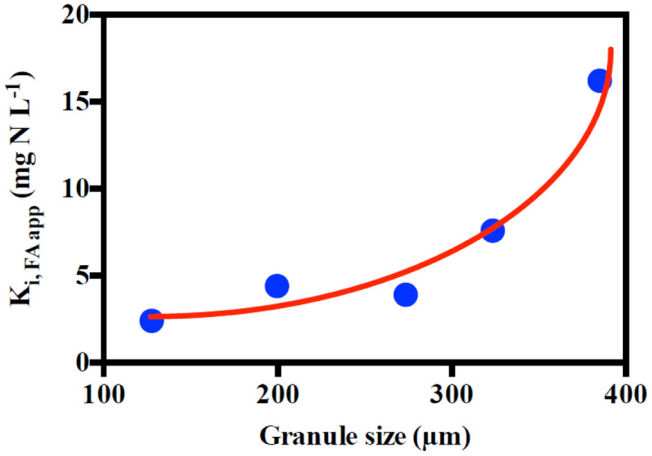

Fig. 5. Experimentally measured apparent FA inhibition coefficient, $K_{I,FAapp}$, for granules of different sizes.

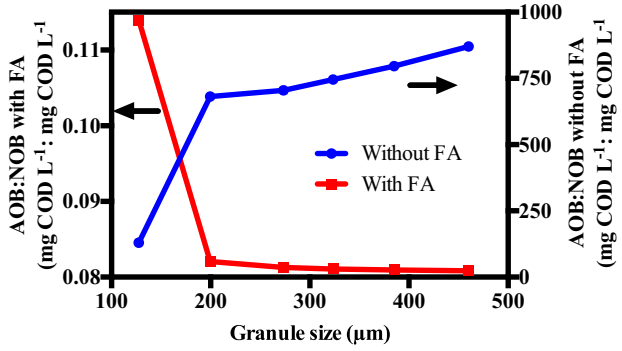

Fig. 6. AOB:NOB abundance ratios for the scenarios with (experimentally measured) and without (model predicted) FA inhibition.

the granule surface can be explained by FA inhibition.

The concentration of FA is determined by three factors in Eq. (6), specifically TAN concentration, temperature, and pH. The decrease in NH_4^+ will tend to also decrease the FA across the granule (Fig. 7). However, according to the study by Poot et al. (2016), pH will have a more significant impact on the decrease in FA than will the drop in NH_4^+. It is expected that pH will decrease in the region of AOB activity since ammonia oxidation releases H^+ ions (Van Hulle et al., 2010). The model predicts such a decline in the pH profile inside the granule structure (Fig. 7). Model predictions in Figs. 7 and 8 suggest that NOB are subjected to the inhibition of FA ranging from 0.5 to 0.58 mg L^{-1}. This is consistent with the results of Anthonisen et al. (1976) who found that the minimum inhibitory value of FA for NOB was in the range of 0.1 to 1 mg FA L^{-1}.

3.6. Model simulation of the specific growth rate distribution of AOB and NOB with and without FA inhibition

Theoretically, the abundance of AOB and NOB is governed by their competition for the limited space within each layer of aerobic granules. Hence, the profiles of their specific growth rate (μ) along the radius of granules of various sizes with and without FA inhibition are simulated in Fig. 9. As can be seen, without FA inhibition, the NOB always grows faster than AOB within the 50 μm top layer of the granule surfaces as a result of the high DO and NO_2^- within this depth (Fig. 7) plus the faster maximum specific growth rate of NOB over AOB, e.g. 0.78 vs. 0.50 d^{-1} (Table S3). That being said, without FA inhibition, there should be more NOB than AOB within aerobic granules, which is in line with numerous observations in literature (Zhu et al., 2018; Winkler et al., 2011). It is noteworthy that this simulation was performed with bulk DO set as low as 0.8 mg L^{-1}, indicating DO control alone is unable to realize long-term mainstream partial nitritation as concluded by other studies (Park et al., 2015; Liu and Wang, 2014). Hence, in order to successfully suppress NOB growth, the effect of FA inhibition has to be taken advantage. Fig. 9 shows that, once the 0.5 to 0.58 mg L^{-1} FA concentration is present (Fig. 7), the specific growth rate of NOB drops significantly below that of the AOB, especially within the top 50 μm layer of the granule surfaces, contributing to the dominance of AOB within this depth (Fig. 8). Yet, beyond this depth, the difference between the specific growth rates of AOB and NOB becomes minor (Fig. 9), which contributes to the increase in the relative abundance of NOB (Fig. 8). Apparently, larger granules tend to cultivate relatively higher abundance of NOB as shown in Fig. 4. Even so, the relative abundance of NOB is still two-order of magnitude lower than that of the AOB (Fig. 8) owing to the effective FA inhibition. Thereby, successful partial nitritation has been achieved in the ALR (Table 1).

3.7. Model simulation of the AOB and NOB distribution and abundance without FA inhibition

The abundance and distribution of AOB and NOB in the smallest (radius of 63.75 μm) and largest (radius of 230 μm) granules without FA inhibition are simulated in Fig. 10 to verify the inference from Fig. 9, i.e. NOB will dominate without FA inhibition. It can be seen that NOB dominates over AOB at the surface of the granules and their abundance shares the same magnitude if FA inhibition is ignored. However, such a situation would not be sustainable since NOB growth would have driven down the NO_2^- concentration over time, leading to a failure of partial nitritation. In other words, NO_2^- accumulation as shown in Table 1 cannot be explained solely by DO limitation. Not only does this situation conflict with the successful partial nitration observed in this study (Table 1), but Fig. 6 also shows that the case without FA inhibition predicts an increasing AOB:NOB ratio with granule size. The experimental data in Fig. 4 is opposite to such a trend, i.e. AOB:NOB decreases as the granule size increases.

4. Discussion

4.1. Effect of granule size on AOB:NOB ratio

Opposing trends can be seen in the literature with regard to the effect of granule size on the AOB:NOB ratio. Analysis of the results from the study by Zhu et al. (2018) indicates that the ratio of AOB:NOB abundance actually increased with increasing granule diameter. NOB became nearly non-existent in aggregates > 50 μm. These results were explained by the researchers as resulting from the competition for limited DO based on relative oxygen affinities (Zhu et al., 2018).

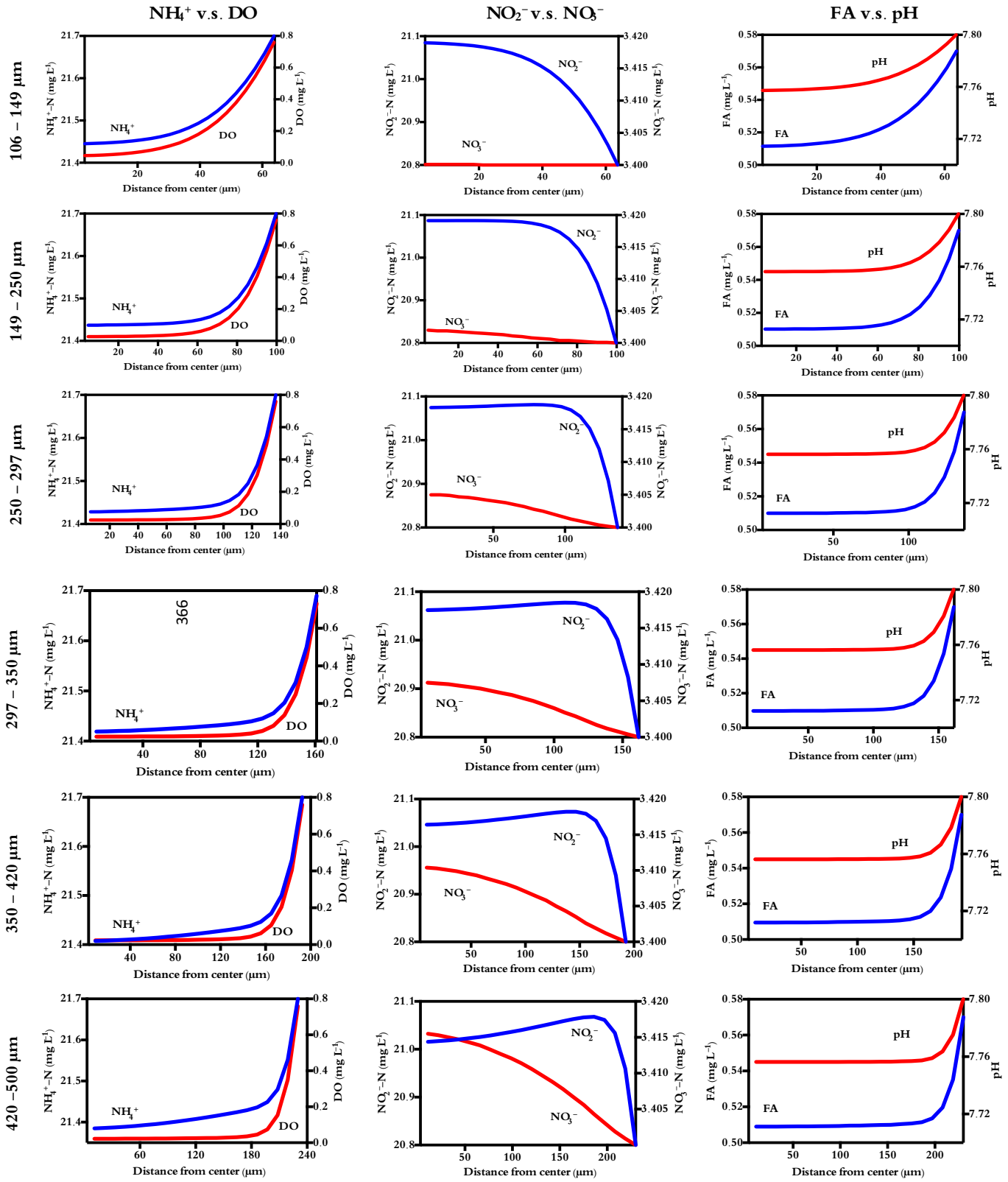

Fig. 7. Model simulated substance profiles along the radius for each granule size range tested.

Winkler et al. (2011) observed the same trend. In fact, Winkler et al. (2011) and Morales et al. (2016) even suggested selectively discarding the smaller aggregates that favor NOB activity. Vlaeminck et al. (2010), however, observed the opposite trend in AOB:NOB activity ratios, with the highest ratio occurring in the smallest granule size. This cannot be explained by DO limitation, so there must be more factors at play. For example, high influent total ammonia nitrogen (TAN) (250–350 mg N L^{-1}) in the study of Vlaeminck et al. (2010) suggests the possibility of FA inhbition. The outcome of this study suggests that FA inhibition might reverse the correlation between the AOB:NOB

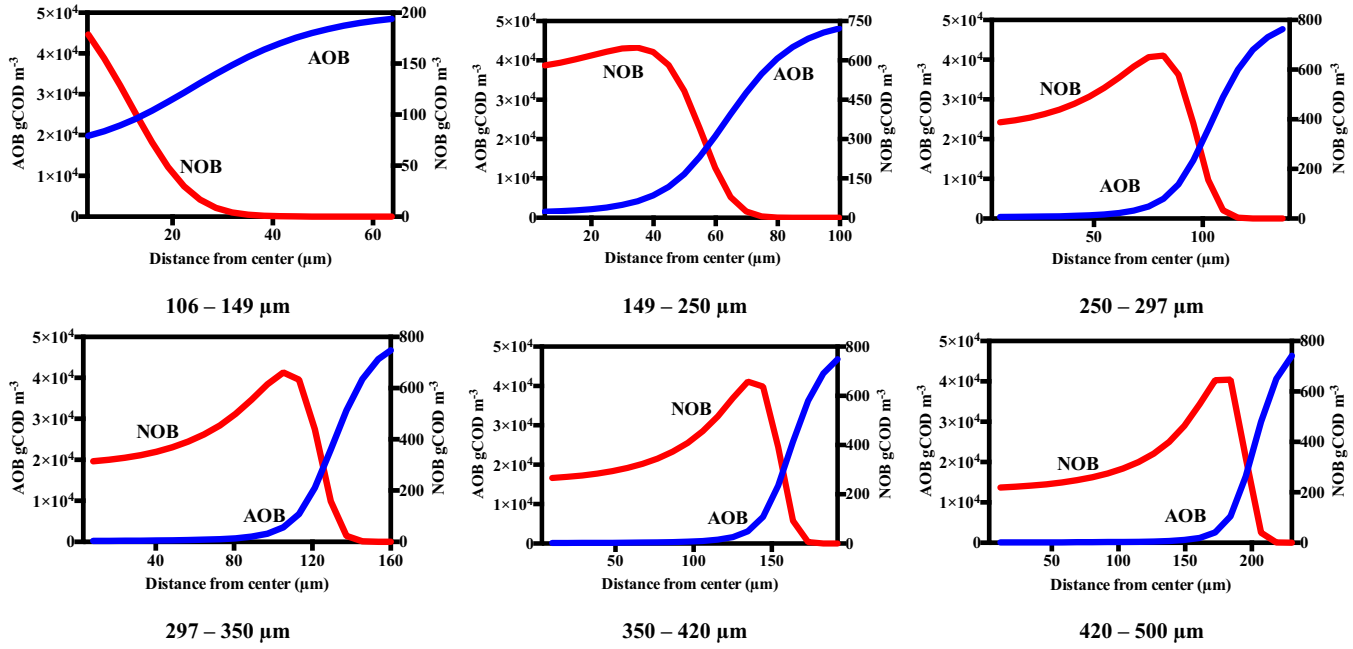

Fig. 8. Model simulated biomass profiles along the radius for each granule size range tested.

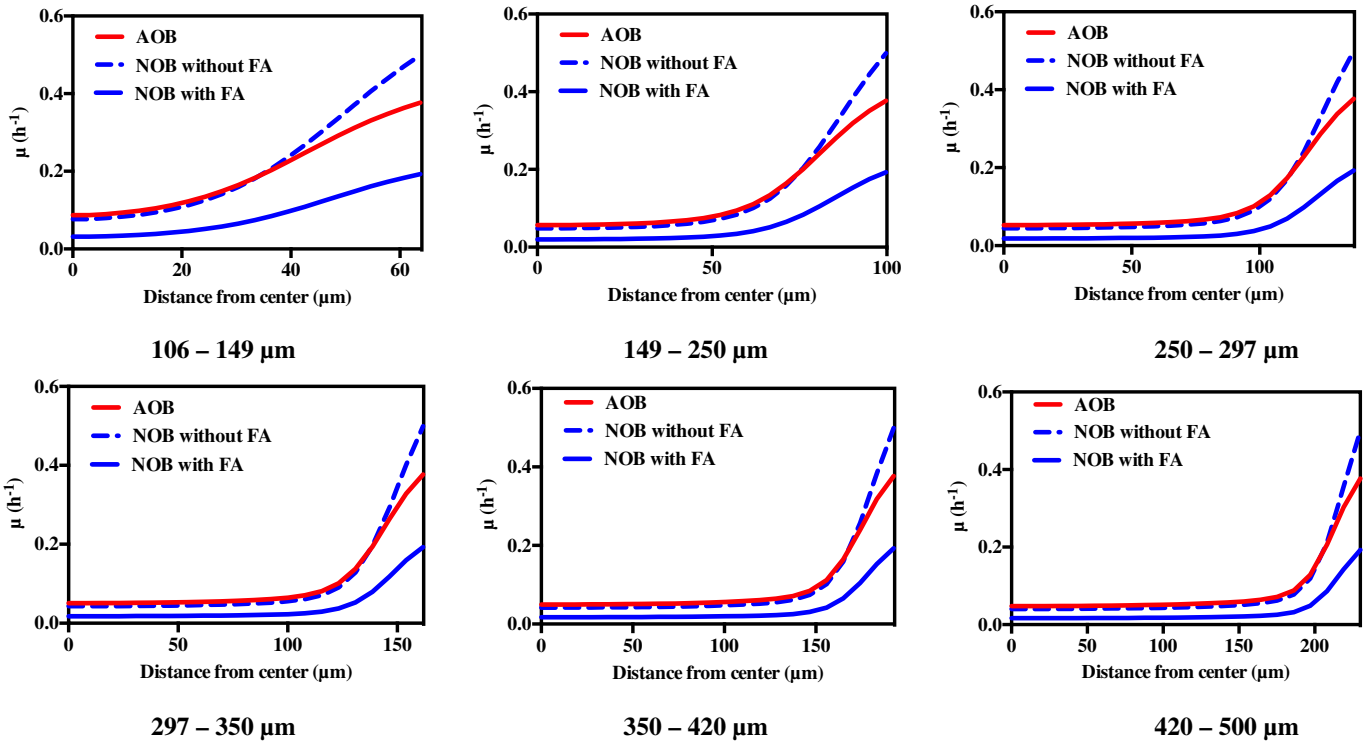

Fig. 9. Model simulated AOB and NOB specific growth rate (μ) profiles along the radius for each granule size range tested.

activity ratio and the granule size, namely more AOB in smaller granules, and vice versa for NOB (Figs. 4 and 6).

4.2. Effect of granule size on the effectiveness of FA inhibition

FA effectively inhibited NOB in the partial nitritation reactor as shown in Table 1. This study demonstrated that FA can have a significant impact on the relative activities of AOB and NOB in granular sludge. Because FA has an inhibitory effect on NOB, the growth rate of NOB becomes smaller than that of the AOB even with sufficient NO_2^- and DO concentrations in the top 50 μm layer of the granules (Figs. 7 and 8). As a consequence, NOB loses the competition with AOB for space in the top layer (Fig. 9). Only when DO concentration becomes very low beneath the 50 μm depth, and AOB's growth slows down, can NOB gain slight growth advantage at around 60 μm beneath the granule surface, where peak NOB abundance is predicted (Fig. 8). This explains the exceptionally high AOB:NOB activity ratio in granules smaller than 60 μm in radii (Fig. 4). In larger granules, the relative growth rates of

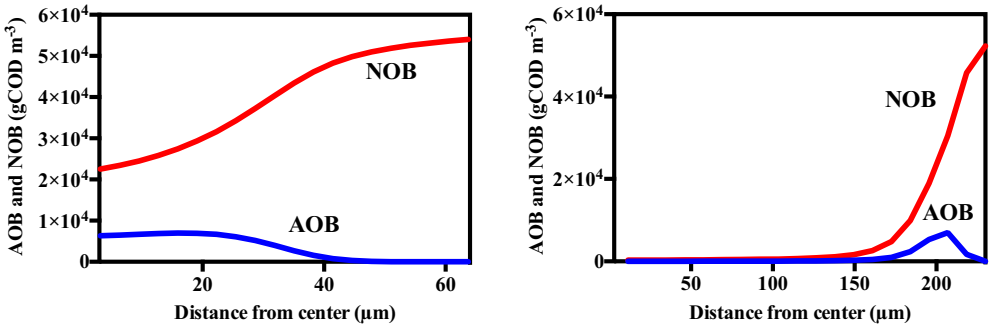

Fig. 10. Model simulated AOB and NOB distribution and abundance in granules with radius of 63.75 μm (left) and 230 μm (right) under the scenario without FA inhibition.

AOB to that of the NOB becomes slightly smaller due to the similar growth rates of AOB and NOB at the depth beneath 50 μm (Fig. 9). Even so, the magnitude of AOB cell abundance is still two magnitudes greater than that of the NOB due to the FA inhibition (Fig. 8). This mass diffusion limitation effect on relative AOB:NOB ratio also can be inferred from the granule size-dependent $K_{I,FAapp}$ values in Fig. 5. Hence, small granules should be selected over larger ones for effective NOB suppression when FA is exploited on the top of the DO control. Since the smallest granules evaluated in this study, i.e. those with diameters in the range of 106–149 μm, showed the least NOB growth, the performance of a partial nitritation reactor may be optimized by supplying a size-based selection pressure such that only smaller granules are retained. This is usually accomplished in the literature with sieves (Kent et al., 2018).

This is contrary to the strategy proposed by Winkler et al. (2011) and Morales et al. (2016), where discarding of smaller aggregates is supposed to favor nitrite accumulation. This is due to the approach used by these researchers in which diffusion-limited oxygen penetration was the only mechanism for suppressing NOB. NOB would be able to grow well in the smaller granules which were fully penetrated by DO, but not in the larger granules where diffusion resistance was significant (Figs. 7 and 8). This is why some studies have observed increasing AOB:NOB ratios with increasing size (Zhu et al., 2018; Winkler et al., 2011). Effluent FA was likely below inhibitory levels in these cases. Analysis of Fig. 6 confirms the conclusion that the AOB:NOB ratio will increase with increasing granule size when FA is non-inhibitory and DO limitation is the only means of NOB suppression; however, AOB:NOB activity ratio will decrease as granules become larger when FA inhibition is present (Figs. 4 and 6). The latter trend, i.e. decreasing AOB:NOB activity ratio with increasing granule size, was also observed by Vlaeminck et al. (2010). Although FA was not considered in that paper and an effluent TAN concentration was not given to compute it, the high influent TAN, i.e. 250–350 mg N L^{-1} and pH of 8 suggest high FA may well have been present in the reactor. FA inhbition, then, is the most likely explanation for the decrease in AOB:NOB ratio, which is consistent with this study.

$K_{I,FAapp}$ values reported in the literature often do not consider the diffusion effect and range from 0.2 (Hiatt and Grady, 2008) to 173 mg N L^{-1} (Gee et al., 1990). The $K_{I,FA}$ regressed in the model in Table S3 was 0.35 mg N L^{-1}, which is on the lower end of the range reported in the literature (Ushiki et al., 2017; Blackburne et al., 2007; Anthonisen et al., 1976; Hiatt and Grady, 2008; Park and Bae, 2009; Li et al., 2011; Wu et al., 2016; Wett and Rauch, 2003; Pambrun et al., 2006; Gee et al., 1990; Gil and Choi, 2001). Since this value represents a true $K_{I,FA}$ with no impact of diffusion on the growth rate of NOB (Eq. (S3)), the low value should be expected. Fig. 5 shows the $K_{I,FAapp}$ for the granule sizes evaluated in this study. These experimentally-measured values were much larger than 0.35 mg N L^{-1}. Thus, $K_{I,FAapp}$ clearly can be seen to increase with granule size, reflecting an increased impact of diffusion resistance. This further supports the conclusion that diffusion limits the effectiveness of FA inhibition of NOB in large granules. Interestingly, the model was found only capable of predicting behavior consistent with the experimental data when FA inhibition of NOB was taken into consideration (Fig. 6), i.e. the model only matched the experimental data when a low $K_{I,FA}$, typical of strong FA inhibition, was regressed.

4.3. Mechanism of NOB suppression in aerobic granules

The key to NOB suppression in granular sludge has often been identified as maintaining a low DO:TAN ratio (Poot et al., 2016; Bartroli et al., 2010). According to this theory, the high TAN concentration accelerates AOB growth, consuming the majority of the oxygen and limiting its availability to NOB (Perez et al., 2009; Poot et al., 2016). Ammonia oxidation, after all, consumes three times as much oxygen compared to nitrite oxidation (Perez et al., 2009; Ma et al., 2016). By applying a low DO:TAN ratio, DO may be significantly limited within the granules even at high bulk DO concentrations. Bartroli et al. (2010), for example, achieved complete suppression of NOB even at DO above 5 mg L^{-1} by maintaining a sufficiently high TAN to set the DO:TAN ratio at 0.18. However, this strategy has the same problem as other strategies solely based on DO limitation, i.e. it depends on the pre-existence of AOB-NOB segregation (Poot et al., 2016). Unless some other mechanism, such as FA inhibition, prevents NOB growth, the presence of high nitrite and DO levels at the surface should be expected to eventually promote nitrite oxidation. However, when TAN is maintained at a high concentration to apply a low DO:TAN ratio, the FA is also potentially high enough to inhibit NOB. FA inhibition was never considered by Poot et al. (2016) who actually achieved pseudo-steady state FA concentrations ranging from 0.02 to 0.54 mg N L^{-1} in the several phases of their experiment. In fact, the FA for much of the experiment was within the minimum inhibitory level range reported by Anthonisen et al. (1976).

The results of this and previous studies, therefore, allow for formulation of a more complete mechanism for NOB suppression. It is likely that neither FA inhibition nor DO limitation is individually capable of completely suppressing nitrite oxidation and the synergistic cooperation of the two is required. The need for this two-pronged approach to successful NOB suppression in granules and biofilms is consistent with the results of two papers from one research group. One of the studies concluded that long-term suppression of nitrite oxidation was not possible with either FA or low DO individually, but was only achieved under a combination of the two (Park et al., 2015). They acknowledged the role of FA, but credited DO as the most important factor for thick, mature biofilms (Park et al., 2010). However, the data in this latter study shows that although low DO decreased the activity of NOB at the biofilm surface, it caused a similar decrease in the growth of AOB. Since the relative activities of AOB and NOB are what truly counts for nitrite accumulation, one would not actually expect this condition to favor nitrite accumulation. It was the other factors, such as pH and FA,

that provided significant activity differences between the two competing groups, showing the importance of FA inhibition at the surface (Fig. 9). A complete mechanism is that FA inhibits NOB at the surface, and DO limitation suppresses its activity in the granule interior (Figs. 7, 8, and 9). This would explain the success that has been observed in the literature by researchers who maintained a low DO:TAN ratio.

5. Conclusions

Following concluding remarks can be drawn from this study:

1. The results of this study imply that FA inhibition in aerobic granules is possible for domestic wastewater with high nitrogen content (50–60 mg NH_4^+-N L^{-1}). However, the ability of FA to inhibit NOB is limited by the relative diffusional resistance inside the granule . Small granules, therefore, are preferred for partial nitritation processes relying on FA for NOB suppression.
2. Diffusion also results in a stratified distribution with AOB dominating in the outer layer and NOB existing only in the granule interior. For effective NOB suppression, however, a low DO must be also maintained inside the granule to limit NOB activity. A model was developed which predicted that NOB suppression would not occur without the influence of FA inhibition. This suggests that FA contributes to the partial nitritation by suppressing NOB at the granule surface.
3. This study is the first to quantify the impact of diffusion on the $K_{I,FAapp}$ of NOB in granular sludge. The influence of diffusion is further manifested by an increasing $K_{I,FAapp}$ as granule size increases. These measured values do not accurately reflect the intrinsic inhibition coefficient, $K_{I,FA}$, but are easy to use and helpful in gaining qualitative insight into the effectiveness of FA inhibition in granular sludge and biofilms.

Acknowledgements

We appreciate VT's OASF support for the publication of this work.

Appendix A. Supplementary data

Supplementary data to this article can be found online at https://doi.org/10.1016/j.envint.2019.105005.

References

Anthonisen, A.C., Loehr, R.C., Prakasam, T.B.S., Srinath, E.G., 1976. Inhibition of nitrification by ammonia and nitrous-acid. J. Water Pollut. Control Fed. 48 (5), 835–852.
Bartroli, A., Perez, J., Carrera, J., 2010. Applying ratio control in a continuous granular reactor to achieve full nitritation under stable operating conditions. Environ. Sci. Technol. 44 (23), 8930–8935.
Blackburne, R., Vadivelu, V.M., Yuan, Z.G., Keller, J., 2007. Kinetic characterisation of an enriched *Nitrospira* culture with comparison to *Nitrobacter*. Water Res. 41 (14), 3033–3042.
Cao, Y.S., van Loosdrecht, M.C.M., Daigger, G.T., 2017. Mainstream partial nitritation-anammox in municipal wastewater treatment: status, bottlenecks, and further studies. Appl. Microbiol. Biotechnol. 101 (4), 1365–1383.
Cui, F., Park, S., Mo, K., Lee, W., Lee, H., Kim, M., 2017. Experimentation and mathematical models for partial nitrification in aerobic granular sludge process. KSCE J. Civ. Eng. 21 (1), 127–133.
Ge, S., Wang, S., Yang, X., Qiu, S., Li, B., Peng, Y., 2015. Detection of nitrifiers and evaluation of partial nitrification for wastewater treatment: a review. Chemosphere 140, 85–98.
Gee, C.S., Suidan, M.T., Pfeffer, J.T., 1990. Modeling of nitrification under substrate-inhibiting conditions. J. Environ. Eng.-ASCE 116 (1), 18–31.
Gil, K.I., Choi, E.S., 2001. Modelling of inhibition of nitrite oxidation in biological nitritation processes by free ammonia. Biotechnol. Lett. 23 (24), 2021–2026.
Grunditz, C., Dalhammar, G., 2001. Development of nitrification inhibition assays using pure cultures of *Nitrosomonas* and *Nitrobacter*. Water Res. 35 (2), 433–440.
Gu, A.Z., Pedros, P.B., Kristiansen, A., Onnis-Hayden, A., Schramm, A., 2007. Nitrifying community analysis in a single submerged attached-growth bioreactor for treatment of high-ammonia waste stream. Water Environ. Res. 79 (13), 2510–2518.
Hao, X., Heijnen, J.J., van Loosdrecht, M.C.M., 2002a. Model-based evaluation of temperature and inflow variations on a partial nitrification–ANAMMOX biofilm process. Water Res. 36, 4839–4849.
Hiatt, W.C., Grady, C.P.L., 2008. An updated process model for carbon oxidation, nitrification, and denitrification. Water Environ. Res. 80 (11), 2145–2156.
Jensen, James N., 2003. A Problem-Solving Approach to Aquatic Chemistry. John Wiley & Sons, Hoboken, NJ.
Kent, T.R., Bott, C.B., Wang, Z., 2018. State of the art of aerobic granulation in continuous flow bioreactors. Biotechnol. Adv. 36 (4), 1139–1166.
Li, X., Sun, Y., Wang, Z.W., He, Z., 2019. Theoretical understanding of the optimum conditions for a mainstream granular nitritation-anammox reactor coupled with anaerobic pretreatment. Sci. Total Environ. 669, 683–691.
Li, Z.R., Zhang, Z., Zhang, Z.J., 2011. Inhibition of nitrification of ammonia-rich wastewater in immobilized nitrifiers system. Adv. Mater. Res-Switz. 183–185 197-200.
Liu, G., Wang, J., 2014. Role of solids retention time on complete nitrification: mechanistic understanding and modeling. J. Environ. Eng. 140 (1), 48–56.
Ma, B., Wang, S., Cao, S., Miao, Y., Jia, F., Du, R., Peng, Y., 2016. Biological nitrogen removal from sewage via anammox: recent advances. Bioresour. Technol. 200, 981–990.
Metcalf and Eddy, 2014. Wastewater Engineering: Treatment and Resource Recovery, fifth ed. McGraw-Hill Education, New York, NY.
Morales, N., del Rio, A., Vazquez-Padin, J.R., Mendez, R., Campos, J.L., Mosquera-Corral, A., 2016. The granular biomass properties and the acclimation period affect the partial nitritation/anammox process stability at a low temperature and ammonium concentration. Process Biochem. 51, 2134–2142.
Moussa, M.S., Lubberding, H.J., Hooijmans, C.M., van Loosdrecht, M.C.M., Gijzen, H.J., 2003. Improved method for determination of ammonia and nitrite oxidation activities in mixed bacterial cultures. Appl. Microbiol. Biotechnol. 63 (2), 217–221.
Nogaj, T.M., Randall, A.A., Jimenez, J.A., Takacs, I., Bott, C.B., Miller, M.W., Murthy, S., Wett, B., 2014. Mathematical modeling of the high rate activated sludge system: optimizing the COD:N ratio in the process effluent. In: Proceedings of WEFTEC 2014, Water Environ Fed, pp. 913–926.
Pambrun, V., Paul, E., Sprandio, M., 2006. Modeling the partial nitrification in sequencing batch reactor for biomass adapted to high ammonia concentrations. Biotechnol. Bioeng. 95 (1), 120–131.
Park, S., Bae, W., 2009. Modeling kinetics of ammonium oxidation and nitrite oxidation under simultaneous inhibition by free ammonia and free nitrous acid. Process Biochem. 44 (6), 631–640.
Park, S., Bae, W., Rittmann, B.E., 2010. Multi-species nitrifying biofilm model (MSNBM) including free ammonia and free nitrous acid inhibition and oxygen limitation. Biotechnol. Bioeng. 105 (6), 1115–1130.
Park, S., Chung, J., Rittmann, B.E., Bae, W., 2015. Nitrite accumulation from simultaneous free-ammonia and free-nitrous-acid inhibition and oxygen limitation in a continuous-flow biofilm reactor. Biotechnol. Bioeng. 112 (1), 43–52.
Perez, J., Costa, E., Kreft, J.U., 2009. Conditions for partial nitrification in biofilm reactors and a kinetic explanation. Biotechnol. Bioeng. 103 (2), 282–295.
Piculell, M., Suarez, C., Li, C., Christensson, M., Persson, F., Wagner, M., Hermansson, M., Jonsson, K., Welander, T., 2016. The inhibitory effects of reject water on nitrifying populations grown at different biofilm thickness. Water Res. 104, 292–302.
Poot, V., Hoekstra, M., Geleijnse, M.A.A., van Loosdrecht, M.C.M., Perez, J., 2016. Effects of the residual ammonium concentration on NOB repression during partial nitritation with granular sludge. Water Res. 106, 518–530.
Reardon, J., Foreman, J.A., Searcy, R.L., 1966. New reactants for the colorimetric determination of ammonia. Clin. Chim. Acta 14, 403–405.
Sen, D., Randall, C.W., 2008. Improved computational model (AQUIFAS) for activated sludge, integrated fixed-film activated sludge, and moving-bed biofilm reactor systems, part II: multilayer biofilm diffusional model. Water Environ. Res. 80 (7), 624–632.
Sun, Y., Angelotti, B., Wang, Z.W., 2019. Continuous-flow aerobic granulation in plug-flow bioreactors fed with real domestic wastewater. Sci. Total Environ. 688, 762–770.
USEPA, 2017. Federal Register. 40 CFR part 136.
Ushiki, N., Jinno, M., Fujitani, H., Suenaga, T., Terada, A., Tsuneda, S., 2017. Nitrite oxidation kinetics of two Nitrospira strains: The quest for competition and ecological niche differentiation. J. Biosci. Bioeng. 123 (5), 581–589.
Van Hulle, S.W.H., Vandeweyer, H.J.P., Meesschaert, B.D., Vanrolleghem, P.A., Dejans, P., Dumoulin, A., 2010. Engineering aspects and practical application of autotrophic nitrogen removal from nitrogen rich streams. Chem. Eng. J. 162, 1–20.
Vlaeminck, S.E., Terada, A., Smets, B.F., De Clippeleir, H., Schaubroeck, T., Bolca, S., Demeestere, L., Mast, J., Boon, N., Carballa, M., Verstraete, W., 2010. Aggregate size and architecture determine microbial activity balance for one-stage partial nitritation and anammox. Appl. Environ. Microbiol. 76 (3), 900–909.
Wei, D., Zhang, K., Ngo, H.H., Guo, W., Wang, S., Li, J., Han, F., Du, B., Wei, Q., 2017. Nitrogen removal via nitrite in a partial nitrification sequencing batch biofilm reactor treating high strength ammonia wastewater and its greenhouse gas emission. Bioresour. Technol. 230, 49–55.
Wei, D., Ngo, H.H., Guo, W., Xu, W., Du, B., Wei, Q., 2018. Partial nitrification granular sludge reactor as a pretreatment for anaerobic ammonium oxidation (Anammox): achievement, performance and microbial community. Bioresour. Technol. 269, 25–31.
Wett, B., Rauch, W., 2003. The role of inorganic carbon limitation in biological nitrogen removal of extremely ammonia concentrated wastewater. Water Res. 37 (5), 1100–1110.
Winkler, M.K.H., Kleerebezem, R., Kuenen, J.G., Yang, J.J., van Loosdrecht, M.C.M., 2011. Segregation of biomass in cyclic anaerobic/aerobic granular sludge allows the enrichment of anaerobic ammonium oxidizing bacteria at low temperatures. Environ. Sci. Technol. 45 (17), 7330–7337.

Wu, J., Zhang, Y., Yan, G., 2016. Differentiating two partial nitrification mechanisms: inhibiting nitrite oxidizing bacteria activity or promoting ammonium oxidizing bacteria activity. J. Environ. Chem. Eng. 4 (3), 3260–3266.
Xu, G.J., Zhou, Y., Yang, Q., Lee, Z.M.P., Gu, J., Lay, W., Cao, Y.S., Liu, Y., 2015. The challenges of mainstream deammonification process for municipal used water treatment. Appl. Microbiol. Biotechnol. 99 (6), 2485–2490.
Zhu, T., Xu, B., Wu, J., 2018. Experimental and mathematical simulation study on the effect of granule particle size distribution on partial nitrification in aerobic granular reactor. Biochem. Eng. J. 134, 22–29.